Control and Optimization of SI-CAI hybrid Combustion Based on Stratified Flame Ignition

Tao Chen[1], Xinyan Wang [2,*], Hua Zhao[1, 2], Hui Xie[1], Bangquan He[1]

1. State Key Laboratory of Engines (SKLE), Tianjin University, China.
2. Centre for Advanced Powertrain and Fuels (CAPF), Brunel University London, UK.

***Corresponding Author:** Xinyan Wang, Centre for Advanced Powertrain and Fuels (CAPF), Brunel University London, UK

Abstract

Spark Ignition (SI)- Controlled Auto-ignition (CAI) Hybrid Combustion (SCHC), also known as Spark Assisted Compression Ignition (SACI), is of considerable interest in gasoline engines because of its potential to enlarge the operating range of gasoline diluted combustion. However, it was found that the SCHC process was often characterized with large cycle-to-cycle variations. In this research, a new approach by combining the traditional second order derivative (SOD) method and Wiebe function fitting method was proposed to identify different heat release stages of SCHC. The heat release characteristics of the SI-CAI hybrid combustion based on Stratified Flame Ignition (SFI) strategy and its control methods were investigated in detail. The effect of control parameters, including spark timing, direct injection ratio and dilution strategy, on improving the thermal efficiency and decreasing the variation of heat release trace in SCHC based on SFI strategy was analysed. The advance of flame propagation ending point (FPE) and the increase of the average heat release rate in flame propagation (FP) stage benefitted the fuel economy and reduced the variations of heat release in SCHC. Although the increase

of direct injection ratio contributed to the stability of heat release in the SCHC based on the SFI strategy, the thermal efficiency of SCHC cannot be effectively optimized due to the decrease of combustion efficiency. The application of exhaust gas recirculation (EGR) and air dilution could decrease the variations of heat release process and increase the thermal efficiency of SCHC based on SFI strategy.

Keywords

SI-CAI hybrid combustion; stratified flame ignition; heat release analysis; cyclic variations; combustion stability control.

1. Introduction

As both emissions standards and fuel consumption legislations become more stringent in the main automotive market of the globe in the upcoming years, advanced combustion technologies are more and more important when attempting to improve the gasoline engine efficiency. The Spark Ignition (SI)- Controlled Auto-ignition (CAI) Hybrid Combustion (SCHC), also known as Spark Assisted Compression Ignition (SACI), proposed in the beginning of this century, is of considerable interest in gasoline engines because of its potential to enlarge the operating range of gasoline combustion compared with Homogeneous Charge Compression Ignition (HCCI) combustion and meanwhile achieve simultaneous reductions in fuel consumption and NO_X emission compared with the traditional SI combustion [1-3].

Previous research has identified two stages of the heat release process in SI-CAI hybrid combustion: spark ignited flame propagation in the first stage and the following auto-ignition

exothermic reactions of unburned mixture [4-8] in the second stage. The understanding and characterization of the two-stage heat release process in SCHC are vital to realise the continuous combustion mode transition by altering the heat release proportion between the flame propagation stage and auto-ignition stage. Compared with the pure CAI combustion, the relatively slow and more reliable initial flame propagation process in SI-CAI hybrid combustion reduces the rate of pressure rise at higher load conditions and improves the ignition stability at lower load conditions [9]. In 2011, Chen et al. [2] applied SCHC to bridge the gaps of temperature and residual gas fraction (RGF) between HCCI combustion and SI combustion and achieved the continuous combustion mode transition with engine load. In the same year, Manofsky et al [8] used a similar method to achieve the simultaneous transition of the engine load and combustion mode.

In order to achieve better control over the combustion process, a greater proportion of spark ignited flame can be employed during the hybrid combustion to achieve smooth heat release process without knocking combustion. With the increase of heat release proportion of flame propagation, the cyclic variations of in-cylinder pressures and heat release rates were observed with the SCHC operations [10-13], and the coefficient of variation (COV) of IMEP could be around 15% [10, 11]. Such large cyclic variations made it difficult to control and optimize the hybrid combustion process at some conditions. In addition to the high cyclic variations, the knock phenomenon at higher loads due to the existence of auto-ignition and misfires at low loads due to high dilution are also challenges of SCHC control. Although the controllability of SCHC has been improved compared with HCCI combustion due to the interaction between initial flame propagation and subsequent auto-ignition, the SCHC control is still influenced

significantly by the combustion boundary conditions. When operating with different gasoline type fuels, Bunting [14] found that the in-cylinder charge temperature and dilution had similar effects on hybrid combustion as on the CAI combustion. Yun et al. [15] found that reducing the residual gas temperature and changing the distribution of residual gas in the cylinder could alter the heat release process of the hybrid combustion and expand the operating range of gasoline high-efficiency low-temperature combustion. Chang et al. [16] proved that the fuel injection during negative valve overlap was an effective way to extend the dilution limit of gasoline hybrid combustion. The work carried out by Polovina et al. [17] and Yang et al. [18] also showed the effectiveness of negative valve overlap (NVO) injection strategy.

However, the aforementioned methods still have the defects of controlling the gasoline SI-CAI hybrid combustion. With the decrease of residual gas fraction (RGF) and the increase of load, the effect of NVO injection strategy would gradually weaken due to less hot residual gas for fuel reforming process [19]. Moreover, Polovina et al. [17] found that the fuel injection during the negative valve overlap resulted in obvious increase in pumping loss. At some operating points, the fuel economy benefit from the improved combustion was less than the increase of pumping loss. Therefore, the method mentioned above which was mainly used to improve the auto-ignition in SCHC would not be effective to control the combustion process in wide operating ranges. At highly diluted conditions, improving the control of flame propagation is more important than that of auto-ignition. Wheeler et al. [20] pointed out that the cooled EGR can cause slower flame propagation, leading to poor engine stability and even misfires. Due to the dilution effect of EGR, both the flame propagation speed and direction varied in continuous cycles of SI-CAI hybrid combustion, which were observed by Xie et al. [21] through

chemiluminescence flame imaging. The instability of flame development and combustion process of SCHC at diluted conditions were caused by some random elements, such as the variations of in-cylinder flow, EGR distribution and temperature distribution [22-24]. In view of the important influence of initial flame propagation on the whole heat release process of SCHC, increasing the flame propagation speed at diluted conditions would be an effective way to reduce the variations of SCHC. In recent years, the stratified flame was seen as an important method to achieve diluted and lean combustion. Shi et al. [25-27] found that the stratified flame could improve the ignition of overall lean charge and increase the flame propagation speed with different fuels through chemical kinetic calculations. In traditional SI combustion, the stratified flame has been thought as an effective way to realize the gasoline lean combustion. In SCHC, the stratified flame could also improve the ignition stability and increase the flame speed through the partially rich charge distribution around the spark plug, which may play a key role on combustion control of SCHC. At high loads, the stratified charge is useful to avoid high pressure rise rate from the auto-ignition of SCHC. The simulation results from Wang et al. [28] showed that the stratified flame could be used to assist the control and stabilisation of the highly diluted gasoline SI-CAI hybrid combustion when the overall charge in the cylinder remained stoichiometric. Compared to the homogeneous SI-CAI hybrid combustion, the key of the stratified flame ignited (SFI) SI-CAI hybrid combustion is the control of in-cylinder fuel distribution. This SFI hybrid combustion could avoid the increase of pumping loss, but heavily depends on the combustion chamber design. Therefore, a new combustion chamber [29] has been designed for the stratified flame ignited SI-CAI hybrid combustion.

In this research, a systematic experimental study was performed to understand the combustion performance of SCHC based on the stratified flame ignition (SFI) strategy. A new approach by combining the traditional second order derivative (SOD) method and Wiebe function fitting method was proposed to identify different heat release stages of SCHC. The heat release characteristics of the SI-CAI hybrid combustion based on Stratified Flame Ignition (SFI) strategy and its control methods were investigated in detail. The effect of control parameters, including spark timing, direct injection ratio and dilution strategy, on improving the thermal efficiency and decreasing the variation of heat release trace in SCHC based on SFI strategy was analysed.

2. Experimental Setup

2.1 Engine specification and test bench

In this research, experiments were carried out in a four-stroke single-cylinder engine and the engine specifications are given in Table 1. The engine comprised a Ricardo Hydra engine block and a specially designed cylinder head equipped with variable valve actuation systems on both intake and exhaust valves. Each system integrated a BMW VANOS variable valve timing device and a BMW Valvetronics continuously variable valve lift device. With the fully variable valve actuation system, intake and exhaust valve lifts can be continuously adjusted from 0.3 mm to 9.5 mm and the valve timings are adjustable within 60 °CA. In order to achieve auto-ignition combustion through trapped residual gases, the intake and exhaust valve profiles were adjusted to achieve negative valve overlaps (NVO).

Table 1. Engine specifications.

Engine type	4 stroke single cylinder
Bore	86 mm
Stroke	86 mm

Displacement	0.5 L
Compression ratio	10.66:1
Combustion chamber	Pent roof / 4 valves
Fuel injection	Port fuel injection
Injection pressure	3 bar
Fuel Gasoline	93 RON
Inlet pressure	Naturally aspirated
Coolant temperature	80 °C
Oil temperature	50 °C

Figure 1 shows the schematic of experimental setup with the control sub-system and the data acquisition sub-system [30]. The engine was connected directly to a 30 kW AC electric dynamometer. A linear oxygen sensor ETAS LA4 (with an accuracy of ±1.5%) was mounted in the exhaust pipe to ensure precise control of the air/fuel ratio. The exhaust gas temperature was measured by a K-type thermocouple installed in the exhaust pipe, which is used to estimate the residual gas fraction in SCHC. At each experimental point, the in-cylinder pressure was measured with a Kistler 6125B piezoelectric transducer and a 5011B charge amplifier. The gaseous exhaust emissions of carbon monoxide (CO), hydrocarbons (HC), and nitrogen oxides (NOx) were measured by a Horiba MEXA-7100 DEGR gas analyzer system. The external exhaust gas recirculation ratio was calculated with the measured concentrations of CO_2 in the exhaust and intake pipes. The mass of the injected fuel by pipe injector per cycle was obtained from the calibration curve between fuel mass and injection pulse width. The total fuel mass was metered by TOCEIL-CMF60. Therefore, the mass of the injected fuel through the direct injector was the difference between the total fuel mass and the fuel mass through the pipe injector.

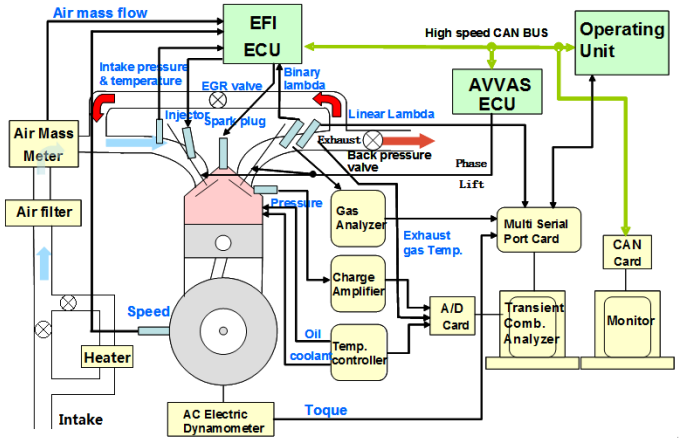

Figure 1. Schematic of the test setup.

2.2 Experimental method

The valve profiles are schematically shown in Figure 2. To achieve the SI-CAI hybrid combustion with the residual gas trapping method, intake and exhaust valve profiles were configured to achieve the negative valve overlap. The exhaust valve parameters were varied according to the requirements of load and dilution level, and the intake valve parameters were used to change the effective compression ratio and decrease the pumping loss. The residual gas fraction (RGF) was calculated by the mass ratio between the in-cylinder residual gas and the total in-cylinder mixture. The in-cylinder residual gas can be predicted by using the state equation of the ideal gas with the exhaust gas temperature and the in-cylinder gas pressure at the exhaust valve closing time. 100 consecutive cycles were used to perform the analysis of the experimental data at each operating point.

The combustion chamber and injector arrangement used in this study were kept as the same with the designs in our previous work [29]. In addition to the low-pressure pipe injection system, a direct injector located bellow the intake pipe was mounted on the cylinder head. The piston, as showed in Figure 3, was redesigned to improve the fuel stratification in the cylinder with the

wall-guided strategy. The gasoline direct injection pressure was fixed at 150 bar in the SFI experiments. The injection timing of direct injection was set as -60 ºCA ATDC based on our previous study [28]. It should be noted that all the crank angle values used in this paper were referenced to combustion top dead centre (TDC). The majority of the fuel was injected in the intake pipe before the open of intake valves through the port injection system. The total amount of fuel injected into the cylinder, including both port injection and direct injection, was fixed around 23.6 mg/cycle with control error within ±1.8% in the experiments. The engine speed was fixed at 1500 r/min during the experiments.

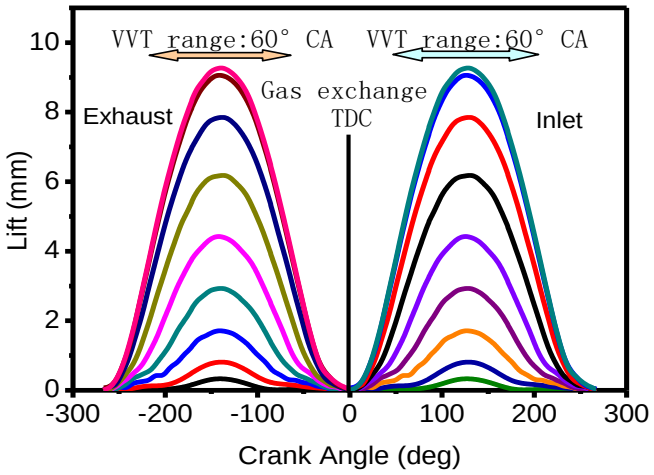

Figure 2. Schematic valve profiles.

Figure 3. The specially designed piston for the SFI strategy.

3. Results and discussion

3.1. Characteristics of SI-CAI hybrid combustion

Figure 4 shows the in-cylinder heat release traces, the statistics of the crank angles at 10%, 50% and 90% burned mass (CA10, CA50 and CA90) and maximum pressure rise rate (MPRR) of 100 consecutive cycles at IMEP 7 bar and 1500 rpm with the negative valve overlap setup. At this operating point, the engine was working at the transition boundary where the dominant combustion mode was changing from multiple auto-ignition to flame propagation mode. As shown in Figure 4 (a), obvious cycle-to-cycle variations of the heat release rate were observed. Both the magnitude and location of the maximum heat release rate varied from cycle to cycle and the oscillation occurred randomly. The statistics of the CA10, CA50, CA90 and MPRR also demonstrated the significant variation of the combustion process of the hybrid combustion at this operating condition. In particular, although the average MPRR was only 1.87 bar/ºCA, the peak MPRR value could achieve at 9.69 bar/ºCA.

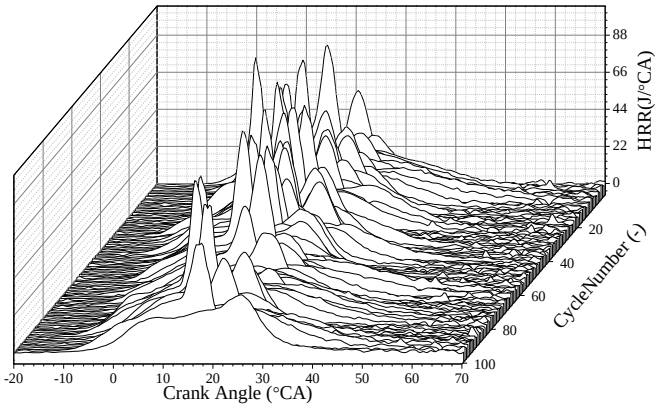

a) heat release rate traces

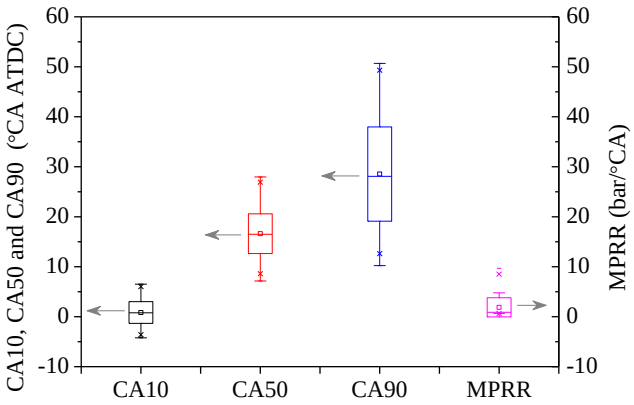

b) CA10, CA50, CA90 and MPRR

Figure 4. Heat release rate traces, CA10, CA50, CA90 and MPRR of 100 consecutive cycles with IMEP = 7 bar and COV_{IMEP}=4.3%.

Based on the observations in Fig.4, the heat release traces can be classified into three groups. In the first group, the cycles with higher maximum heat release rate (MHRR) were characterised with the most advanced timing of MHRR and higher maximum pressure rise rate (MPRR). In the second group, as the MHRR decreased, the timing of MHRR was delayed with the acceptable MPRR. For the remaining cycles in the third group, the heat release process was smooth without any abrupt change, indicating the disappearance of the auto-ignition mode. Apparently, the combustion cycles were not favourable in the first and third groups due to the unacceptable MPRR and low efficiency respectively. Although advancing the spark timing would optimize the combustion phasing of the cycles in the third group, this also led to serious knocking combustion in some other cycles. In contrast, delaying the spark timing can be used to suppress the knocking combustion in the first group, but the overall combustion phasing was shifted away from the optimized value, leading to lower thermal efficiency. This phenomenon is the main challenge for the application of SCHC, which has been found and analysed in our

previous work [13]. Actually, the SFI strategy was proposed to enhance the combustion control and avoid this phenomenon.

The evaluation of the cycle-to-cycle variations of the heat release process is important to explore the combustion control strategies. In order to overcome the difficulty of the method with second order derivative (SOD) of the heat release rate profile, a method based on the Wiebe function fitting was developed by Chen et al. [13] to identify the contribution of auto-ignition combustion in the SI-CAI hybrid combustion mode. In order to effectively evaluate the SFI strategy, a new analytical approach was developed in this study based on the three-stage heat release assumption to quantify the heat release stages of SI-CAI hybrid combustion. Figure 5 shows a typical heat release rate curve of the SCHC with different combustion stages based on the proposed three-stage heat release assumption. In the first combustion stage, the flame propagation combustion can be observed. It should be noted that the combustion process in the second stage varied case to case and the corresponding heat release rate could be accelerated, decelerated or kept constant. In the third stage, a visible heat release rate peak just like CAI combustion may be observed. But the third stage didn’t always exist in SCHC. In order to identify these combustion stages, the new evaluation method should be able to distinguish different stages with clear transition points between different heat release stages based on the heat release trace of SCHC.

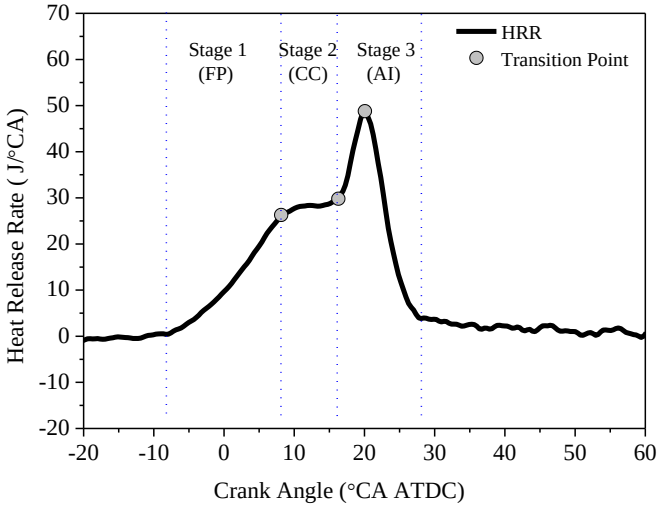

Figure 5. Typical heat release rate curve of the SCHC with different combustion stages.

As the heat release rate in SCHC can be disturbed due to the pressure oscillation, the second order derivative (SOD) method is ineffective for the SCHC. In terms of the Wiebe function fitting method, the transition point is calculated by identifying the timing when the actual heat release trace differs from the Wiebe function fitting curve with a difference value. Therefore, the Wiebe function fitting method is also difficult to obtain the accurate transition points because the selection of the difference value is ambiguous and could directly affect the results. Although the above two methods have their own defects, the blend of above two methods, named as blend method (BM) in this study, could be an effective way to trace the heat release process of SCHC and predict the characteristic transition points. In the proposed blend method (BM), the Wiebe function fitting method was used to seek the scope of transition points while the SOD method was used to scan the local extreme point within this scope. Based on the three-stage heat release assumption and the obtained transition points, the total heat release process can be separated into flame propagation (FP) stage, complex combustion (CC) stage and auto-ignition (AI) dominated stage. Although the CC and AI stages didn't exist in some cycles, they were assumed to exist at the beginning with the blend method. The existence of the CC and AI stages

will then be judged by the relationship between the predicted transition points. The calculation method is detailed as following.

Firstly, calculate the second derivative curve of the heat release rate curve.

Secondly, fit the real heat release trace from spark timing (ST) to the crank angle at 10% burned mass (CA10) based on the Wiebe function [13]. There are three important terms used in the Wiebe fitting process of the heat release rate. The first term is the real heat release trace, which was calculated from the measured pressure trace in the experiments. The second term is the fitting curve, which was calculated based on the Wiebe fitting of the real heat release trace for a certain period (e.g. ST to CA10). The fitting curve outside this period used for the Wiebe fitting (e.g. later than CA10) gradually deviated with the real heat release rate. Therefore, the third term, i.e. the fitting difference ratio, was defined as the ratio of the absolute difference between the real heat release trace and fitting curve to the real heat release rate at a certain crank angle.

Thirdly, identify the crank angle where the fitting difference ratio reached 5% as the reference point #1. The period from 1.08 ºCA before the reference point #1 to 1.8 ºCA after the reference point #1 was then assumed as the searching scope. The crank angle with the minimum second derivative within this searching scope was defined as the first characteristic point, i.e. flame propagation ending point (FPE).

Fourthly, fit the heat release trace from the crank angle at 85% burned mass (CA85) to the crank angle at 95% burned mass (CA95) based on the Wiebe function. The crank angle where the fitting difference ratio reached 5% was identified as reference point #2 by searching backward from CA85. Then, the second searching scope was set from 1.8 ºCA before the

reference point #2 to 1.08 ºCA after this reference point. The crank angle with the minimum second derivative in the second search scope was defined as the second characteristic point, i.e. auto-ignition peak (AIP) point.

Fifthly, traverse the second derivative curve from PFE to AIP and identify the crank angle with the maximum value as the third characteristic point, i.e. auto-ignition beginning (AIB) point.

Sixth, classify the combustion stages based on the above characteristic points. If the FPE couldn't be identified, or the AIP was earlier than FPE, the whole combustion process was merged into a unity, just like the pure SI combustion or CAI combustion. If the maximum second derivative value of the AIB was less than 0.2, there was no auto-ignition dominated stage and the whole heat release process would be classified into two stages, i.e. FP and CC. If the absolute value of the second derivative of FPE was less than 0.2, indicating a small change of heat release rate between the FP and CC stage, the FP and CC could be merged as the FP stage. At last, if no characteristic point was identified, the whole heat release trace was treated as one stage.

The classification of a typical heat release curve based on the three-stage assumption with the proposed BM is shown in Figure 6, and typical heat release curves with merged stages (single-stage and two-stage) are shown in Figure 7. As shown in Figures 6 and 7, the red curve was the Wiebe fitting curve of the real heat release rate based on the period from ST to CA10. The blue curve was the Wiebe fitting curve of the real heat release rate based on the period from CA85 to CA95. Different combustion stages of the SCHC can be identified clearly at different

conditions by the proposed blend method (BM). The effect of SFI strategy on SCHC control will then be analysed in detail with this method.

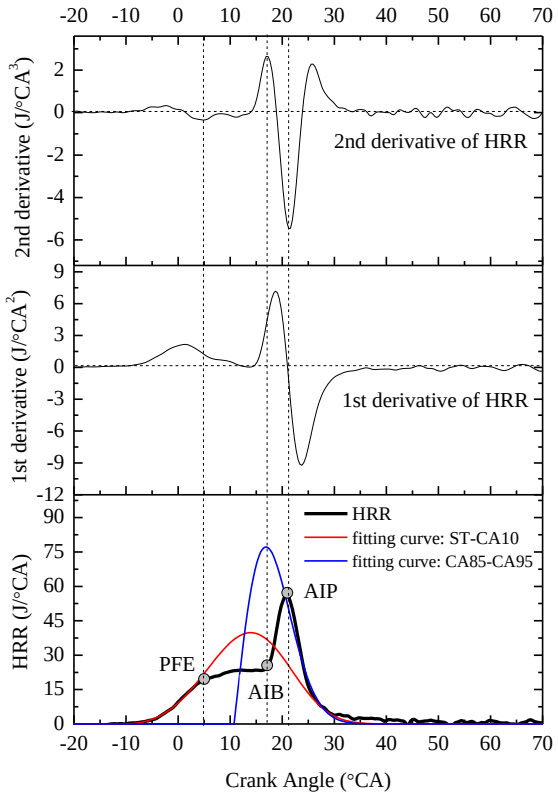

Figure 6. Classification of a typical heat release trace with three combustion stages by the proposed BM.

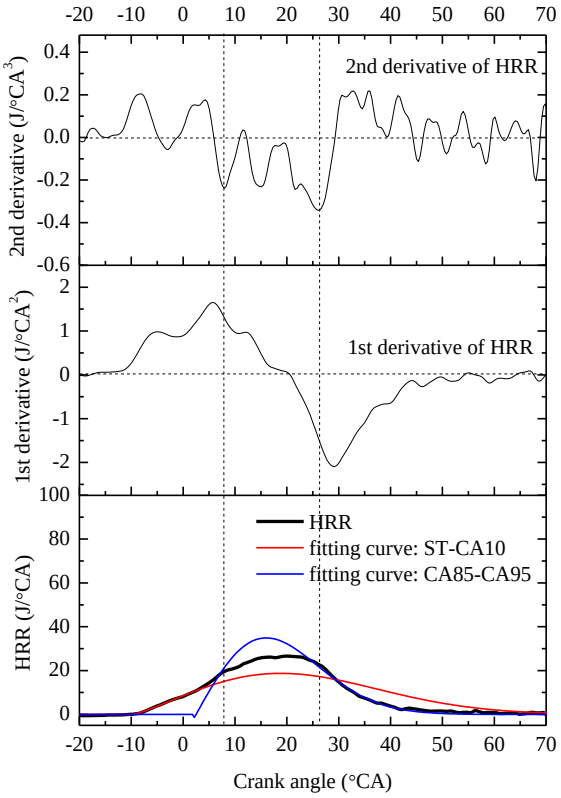

a) Two-stage heat release

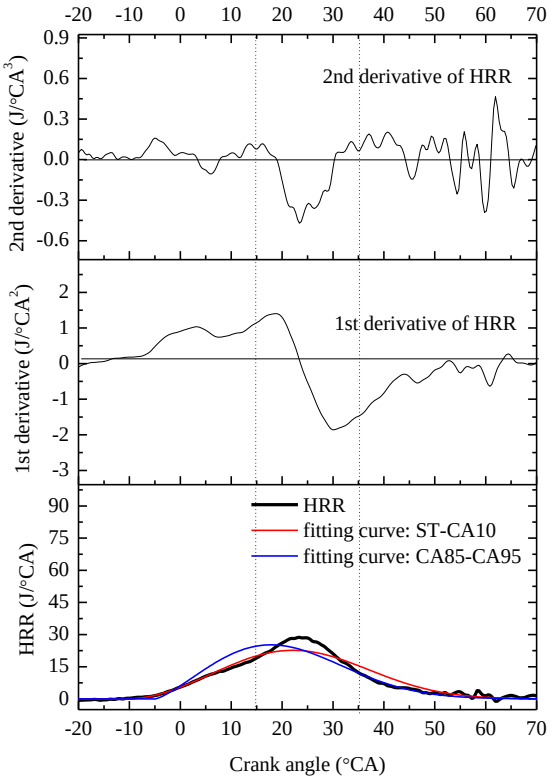

b) Single-stage heat release

Figure 7. Classification of typical heat release curves with merged stages.

3.2 Effect of SFI strategy on SCHC at stoichiometric condition

3.2.1 Effect of spark timing on SCHC combustion

In SFI strategy, the in-cylinder fuel stratification relied on the mixing process of the directly injected fuel and in-cylinder charge, which determined the suitable spark timing window. The effect of spark timing on the combustion process was studied with the direct injection ratio of 28% and direct injection timing at 60 ºCA BTDC. As shown in Fig.8, the CA10 was delayed linearly with the postpone of spark timing and the combustion duration was increased from 19 ºCA to 36 ºCA correspondingly. Meanwhile, the IMEP showed a decreasing trend with the delay of spark timing and the coefficient of variation (COV) of IMEP was also increased. It should be noted that the COV of IMEP of 5% was set as the limit of combustion instability in this study.

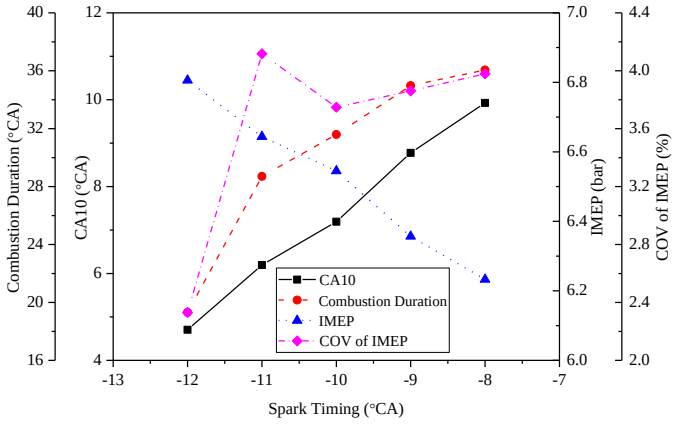

Figure 8. The effect of spark timing on CA10, combustion duration, IMEP and COV of IMEP with SFI strategy.

The conventional knock criterion, such as the averaged maximum pressure rise rate (MPRR) of 100 consecutive cycle below 5 bar/ºCA, was hard to describe the knock phenomenon in SCHC due to the strong variations of combustion process. Although the mean value of MPRR can be kept below 5 bar/ºCA at a specific operating point, the MPRR of some extreme cycles

can reach or considerably exceed 5 bar/ºCA due to high CCVs. In order to accurately reflect the knock phenomenon of SCHC, the mean MPRR of top 50 cycles in 100 consecutive cycles was chosen as a new criterion of knock phenomenon. Figure 9 shows the effect of spark timing on MPRR, mean MPRR of top 50 cycles and the COV of MPRR. With the spark timing at -12 ºCA ATDC, the mean value of MPRR was only 1.6 bar/ºCA, while the mean MPRR of top 50 cycles reached 9.7 bar/ºCA. At this operating point, the COV of MPRR also reached 80%. For a normal gasoline engine, the high MPRR over 10 bar/ºCA could destroy the engine and cause the safety problems. Therefore, in this study, the mean MPRR of top 50 cycles (Top50 MPRR) was controlled below 5 bar/ºCA and the maximum MPRR in 100 consecutive cycles was also controlled below 10 bar/ºCA in the meantime. These two criteria were used as the knock limit in this research. As expected, the top50 MPRR decreased with the delay of spark timing and the spark timing from -11 to -8 ºCA ATDC were acceptable in terms of the knock. Considering the fuel efficiency, as indicated by the IMEP values in Figure 8, the spark timing at -11 ºCA ATDC was the best choice at this operating point.

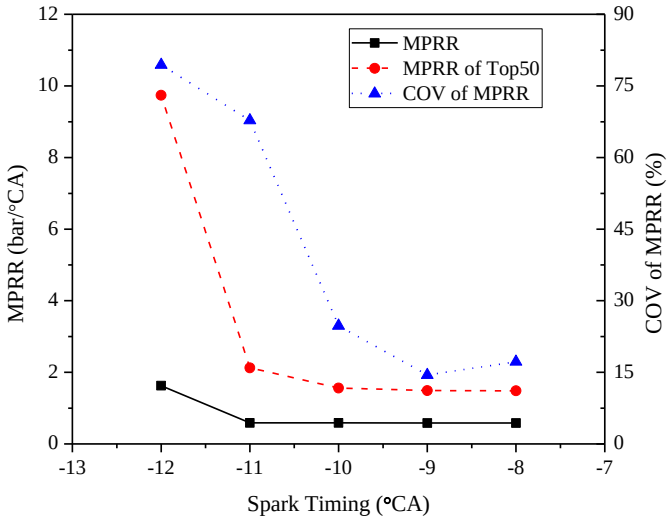

Figure 9. The effect of spark timing on MPRR, mean MPRR of top 50 cycles and the COV of MPRR with SFI strategy.

Figure 10 shows the numbers of cycles with different heat release stages in 100 consecutive cycles with the delay of spark timing. As shown in the figure, most of the combustion cycles had three combustion stages with the spark ignition timing at -12 ºCA ATDC. Therefore, more cycles with an auto-ignition stage in SCHC could lead to unacceptable MPRR and knocking combustion at this operating point. With the delay of spark timing, the number of cycles with single heat release stage gradually increased, indicating increased proportion of slow flame propagation combustion. The numbers of one-stage, two-stage and three-stage heat release cycles were similar in 100 consecutive cycles with the spark timing at -8 ºCA ATDC, indicating higher variations of heat release process among different cycles.

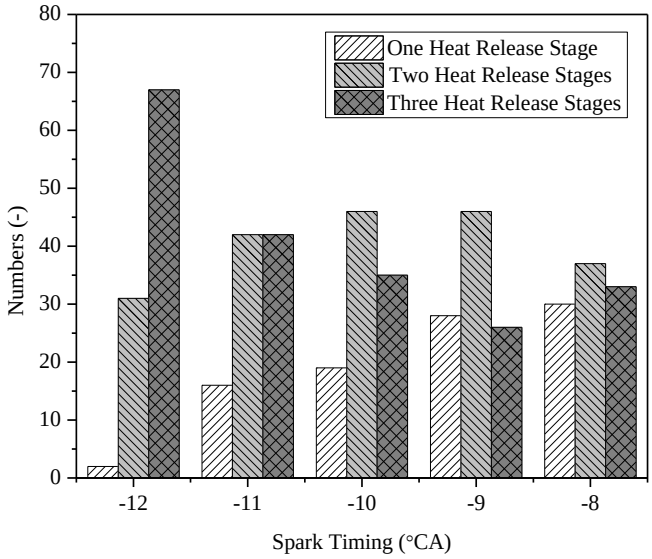

Figure 10. The numbers of cycles with different heat release stages in 100 consecutive cycles with the delay of spark timing.

Overall, the CA50 and IMEP showed strong negative correlation, as shown in Figure 11. As the fuel amount was fixed in this study, a lower IMEP indicated poorer fuel economy. However, it was noted that the correlation became weaker with the earliest spark timing at -12 ºCA ATDC.

Therefore, CA50 was not an effective index to evaluate the fuel consumption of SCHC at the near-knock boundary with early spark timings.

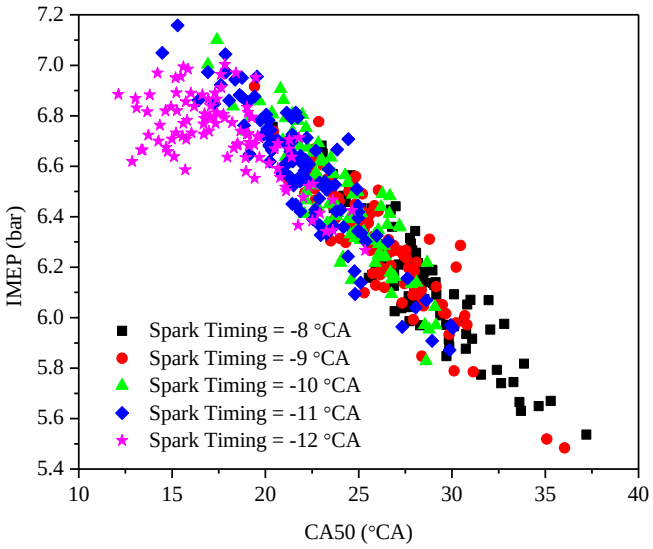

Figure 11. The relationship between CA50 and IMEP in SCHC.

Improving the fuel consumption of stable combustion without knock is the key in the combustion optimization of SCHC based on SFI strategy. Figure 12 shows the contour maps of IMPE against the crank angles of FPE points and average heat release rates in FP stage at different spark timings. The crank angle of FPE point was obtained through the aforementioned blend method. The average heat release rate in FP stage was calculated by dividing the total heat release in FP stage by the duration of FP stage. As shown in Fig. 12, the advance of FPE point and increase of average heat release rate in FP stage could produce higher IMEPs. The highest IMEP can always be found at the upper boundary at each spark timing. As the spark timing delayed from -12 ºCA in Fig 12 (a) to -8 ºCA in Fig. 12 (e), the whole contour map moved toward the bottom right corner, accounting for the lower fuel economy with later spark timings. The first order fitting function was used to evaluate the effect of FPE point and average heat release rate in FP stage based on the data presented in Fig. 12:

$$\mathrm{IMEP} = 6.033 - 0.59882 \times \mathrm{FPE} + 0.1125 \times \mathrm{FPR},\ R^2 = 0.81 \quad (1)$$

The parameters FPE and FPR represented the FPE point and average heat release rate in FP stage respectively. The fitting equation indicated that an earlier transition from flame propagation to complex combustion (CC) or auto-ignition (AI) dominated stage with higher flame propagation rate in FP stage could improve the thermal efficiency of SCHC. Actually, the increase of the flame propagation rate in FP stage was beneficial to advance the transition from FP to CC or AI and decrease the number of cycles with single heat release stage. However, an earlier FPE point and a higher average heat release rate in FP stage could also lead to unacceptable MPRR. Therefore, for better fuel economy, the improvement of SCHC based on SFI strategy should focus on advancing the FPE point and raising the heat release rate in FP stage but avoiding the knock.

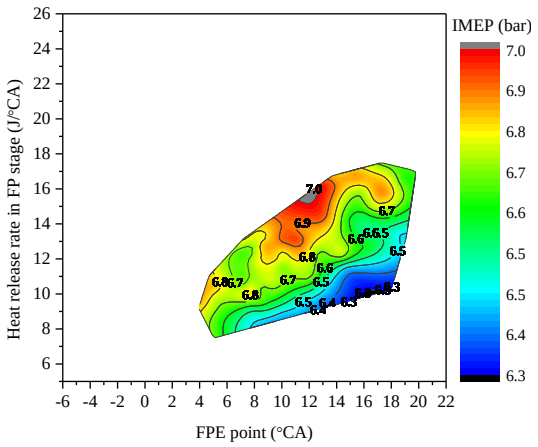

a) Spark timing at -12 ºCA ATDC

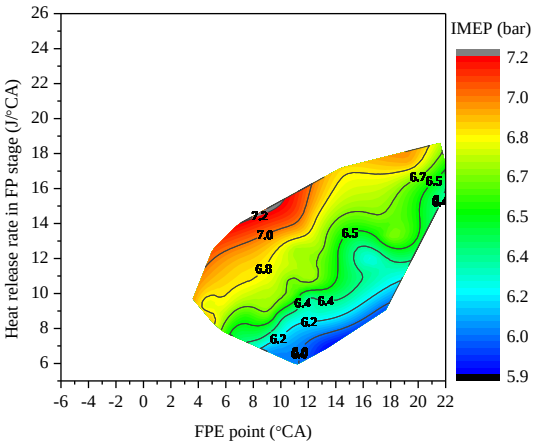

b) Spark timing at -11 ºCA ATDC

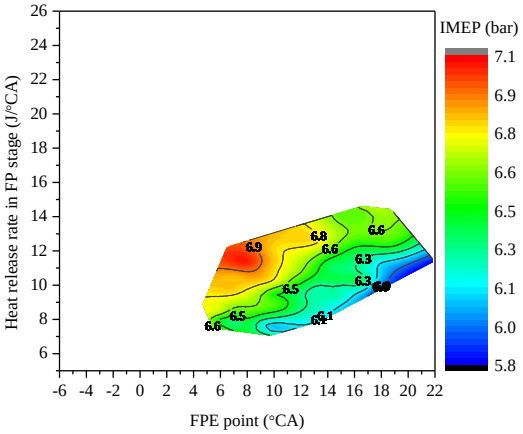

c) Spark timing at -10 ºCA ATDC

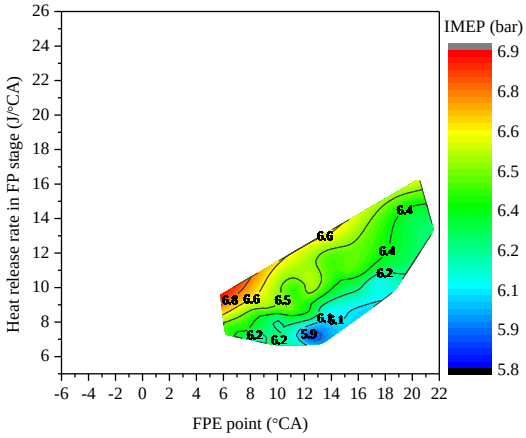

d) Spark timing at -9 ºCA ATDC

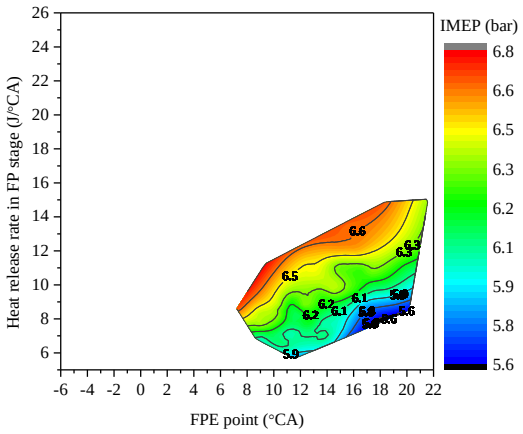

e) Spark timing at -8 ºCA ATDC

Figure12. Contour maps of IMEP against the crank angles of FPE points and average heat release rates in FP stage.

3.2.2 Optimization of direct injection ratio

The basic concept of SFI strategy was to speed up the initial flame propagation by introducing the stratified fuel/air mixture around the spark plug. The amount of direct injected fuel was an important parameter influencing the fuel stratification in the cylinder. Therefore, the effect of direct injection ratio on SCHC was investigated with the optimal spark timing at each operating point. The Top50 MPRR was controlled below 5 bar/ºCA and MPRR below 10 bar/ºCA.

Figure 13 shows the effect of direct injection ratio on the optimal spark timing and MPRR. The optimal spark timing was advanced with the increase of direct injection ratio due to the increased fuel stratification. The higher heat release rate in the auto-ignition dominated stage usually was the reason of high pressure rise rate in SCHC. As the overall lambda in the cylinder was fixed at stoichiometry, the increase of direct injection rate led to higher fuel stratification with richer mixture around the spark plug while leaner mixture at the outer region, which weakened the heat release from the auto-ignition stage. This can be further evidenced by the decreased Top50 MPRR when the direct injection ratio increased from 8% to 18% at the same

spark timing. Similar phenomenon can also be observed when the direct injection ratio increased from 28% to 38%. Therefore, the increase of the direct injection ratio could effectively prohibit the occurrence of knock and enable the advance of spark timing to improve the combustion phasing.

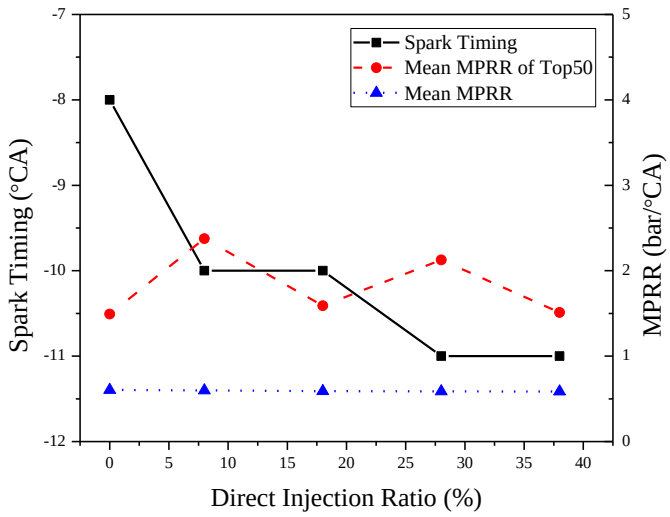

Figure 13. The effect of direct injection ratio on the optimal spark timing and MPRR.

Figure 14 shows the effect of direct injection ratio on CA10, combustion duration, IMEP and COV of IMEP. The spark timing with SFI strategy can be advanced to optimize the combustion performance, leading to earlier CA10 than that in homogeneous case with direct injection ratio of 0. The direct injection ratio of 28% produced earlies CA10. However, the further increase of the direct injection ratio to 38% led to slightly delayed CA10, indicating slower flame propagation with over-stratified charge. Meanwhile, the combustion duration showed a decreasing trend when the direct injection ratio increased from 0 to 28%. The further increase of direct injection ratio to 38% led to slightly longer combustion duration due to slowed flame propagation process. The IMEP showed a decreasing trend with the direct injection ratio, which was mainly caused by the reduction of combustion efficiency due to the increased fuel

stratification. In terms of the cyclic variations, the minimum COV of IMEP was achieved when the direct injection ratio was kept at 18%. The further increase of direct injection ratio could lead to higher COV of IMEP. Therefore, although SFI strategy was capable to increase IMEP and reduce COV of IMEP compared to the homogeneous case, the direct injection ratio should be well controlled in order to achieve these improvements.

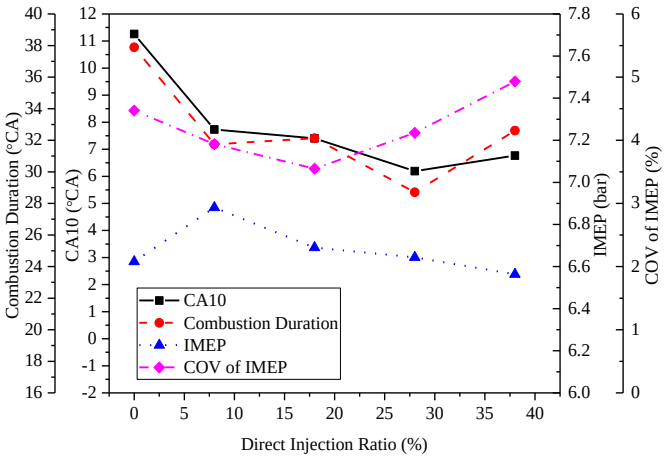

Figure 14. The effect of direct injection ratio on CA10, combustion duration, IMEP and COV of IMEP.

Figure15 shows the effect of direct injection ratio on mean total heat release per cycle, CO and NO_X emissions. Although the SFI strategy improved the combustion phasing and decreased the combustion duration, the CO emission increased significantly with the direct injection ratio due to the local rich zone of the stratified fuel around the spark plug, leading to lower combustion efficiency. It was further evidenced by the gradually reduction of total heat release with the direct injection ratio in Fig.15. The reduction of the total heat release due to the stratified charge counteracted with the benefits from the optimized combustion phasing with SFI strategy. On the other hand, the in-cylinder temperature was also decreased with the direct injection ratio due to the charge cooling effect and reduced total heat release, leading to reduced NOx emission. When the direct injection ratio reached 38%, the NOx emissions in exhaust gas had

dropped down to 510 ppm. In addition, the reduction of in-cylinder temperature would also decrease the heat transfer loss, leading to the improvement of thermal efficiency. It should be noted that the total heat release in Fig. 15 was calculated by the integral of heat release rate curve based on the first law of thermodynamics, which had excluded the heat transfer loss. Therefore, the increase of total heat release with the direct injection ratio at 38% could be caused by the reduction of heat transfer loss. In general, the effectiveness of SFI strategy would be influenced by combustion phasing optimization, combustion temperature and combustion efficiency.

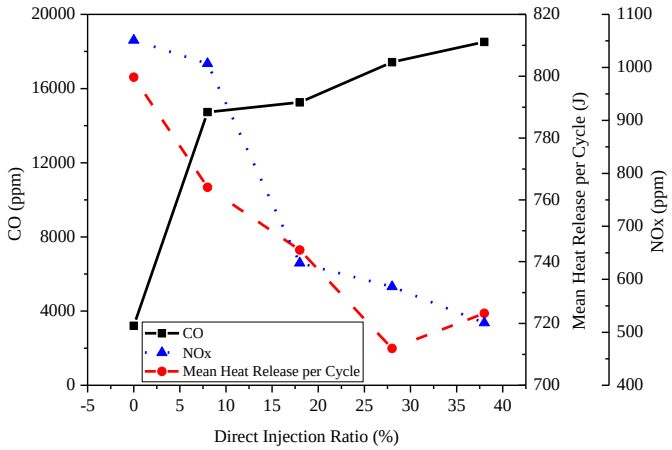

Figure 15. The effect of direct injection ratio on mean total heat release per cycle, CO and NO_X emissions.

Figure 16 shows the contour maps of IMEP against the crank angles of FPE points and average heat release rates in FP stage. As shown in Fig. 16 (a), the contour map of IMEP located at the bottom right corner with late FPE points and low heat release rates in FP stage when the direct injection ratio was kept at 0 (homogeneous case). Figure 16 (b-e) clearly shows that the application of the SFI strategy successfully expanded the entire contour map of IMEP toward earlier FPE points and higher heat release rates in FP stage. In addition to the expanded

operating ranges of the SCHC, it was also found that the application of SFI strategy produced higher maximum IMEPs at the upper boundary of the contour map with much earlier PFE points.

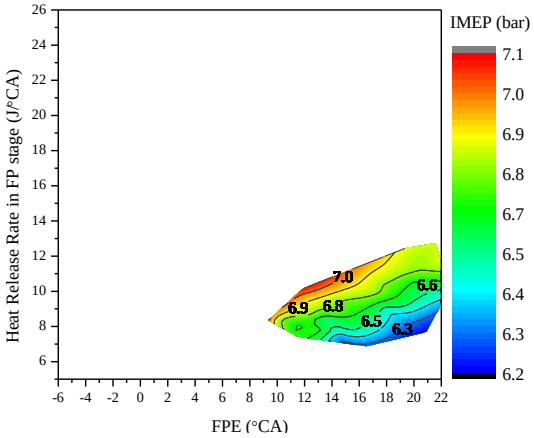

a) Direct injection ratio of 0 (homogenous case)

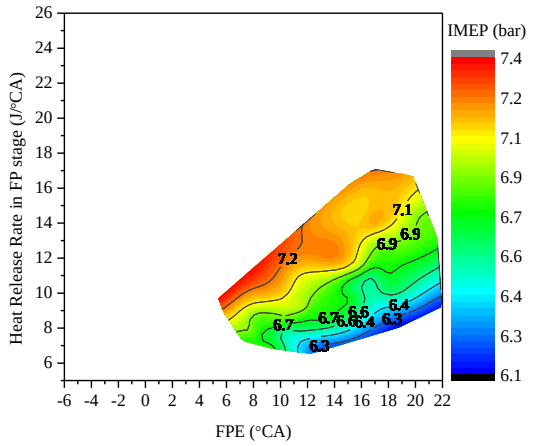

b) Direct injection ratio of 8%

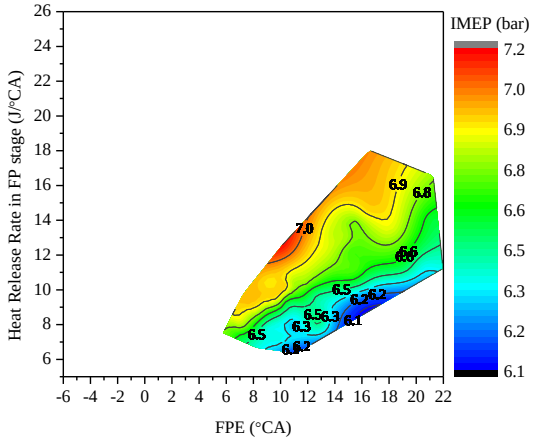

c) Direct injection ratio of 18%

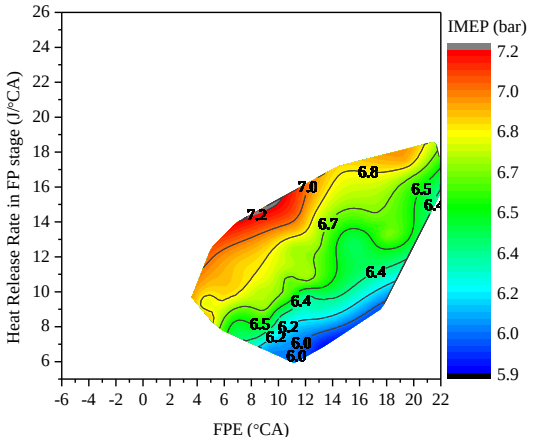

d) Direct injection ratio of 28%

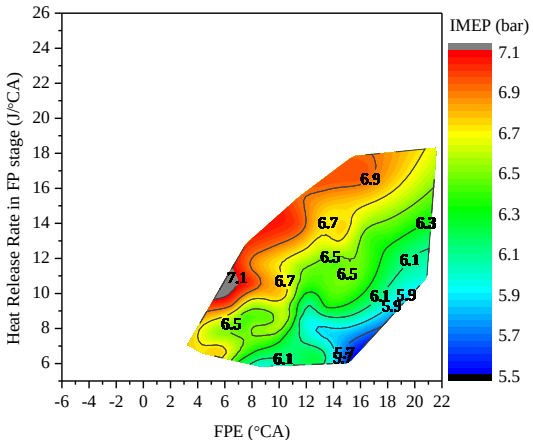

e) Direct injection ratio of 38%

Figure16. Effect of direct injection ratio on the contour maps of IMEP against the crank angles of FPE points and average heat release rates in FP stage.

Figure 17 shows the statistic information of the FPE points and the heat release rates in FP stage with different direct injection ratios. As shown in Fig. 17 (a), the increased direct injection ratio advanced the FPE point and advanced the entire Interquartile Range (IQR) due to the advance of spark timing. Both the mean and median values of the crank angles of FPE points were advanced with the direct injection ratio. However, the variation of the average heat release rates in FP stage was relatively complicated. The SFI strategy led to larger variations of the

average heat release rates in FP stage with the increase of direct injection ratio, as indicated by the wider Interquartile Range (IQR) with the direct injections.

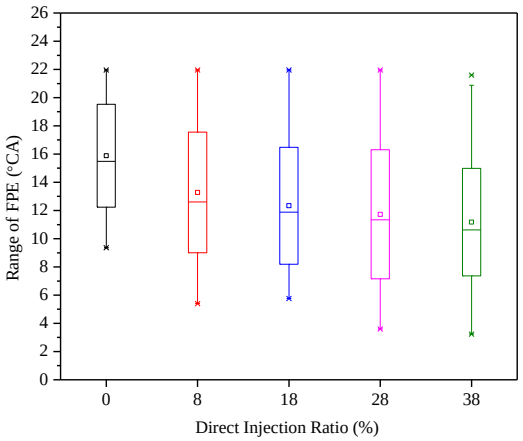

a) crank angles of FPE points

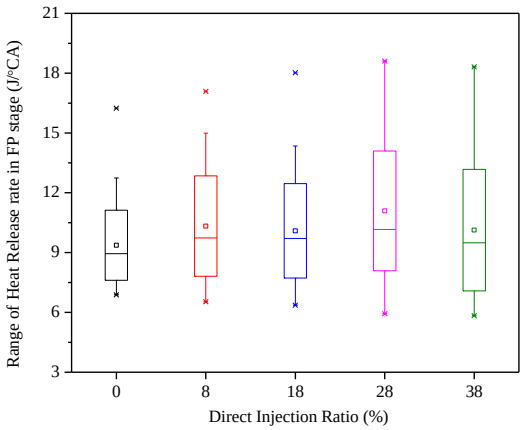

b) average heat release rates in FP stage

Figure 17. The statistic information of the FPE points and the heat release rates in FP stage with different direct injection ratios.

Figure 18 shows the variations of heat release stages with different direct injection ratios. The SFI strategy produced less cycles with 1-stage heat release but more cycles with 2-stage and 3-stage heat release than the homogenous case, indicating higher proportion of auto-ignition combustion in SCHC with SFI strategy. However, the thermal efficiency, as indicated by the

IMEPs in Figures 14 and 16, were not significantly increased especially with a large direct injection ratio due to the decrease of total heat release.

Overall, the SFI strategy was an effective method to improve the combustion phasing of SCHC. Increasing the direct injection ratio was beneficial to trigger auto-ignition in SCHC and decrease the number of the cycles with 1-stage heat release. However, it was also found that the over-stratified fuel distribution led to deteriorated combustion efficiency with a high direct injection ratio and showed little improvement of thermal efficiency at the overall stoichiometric condition.

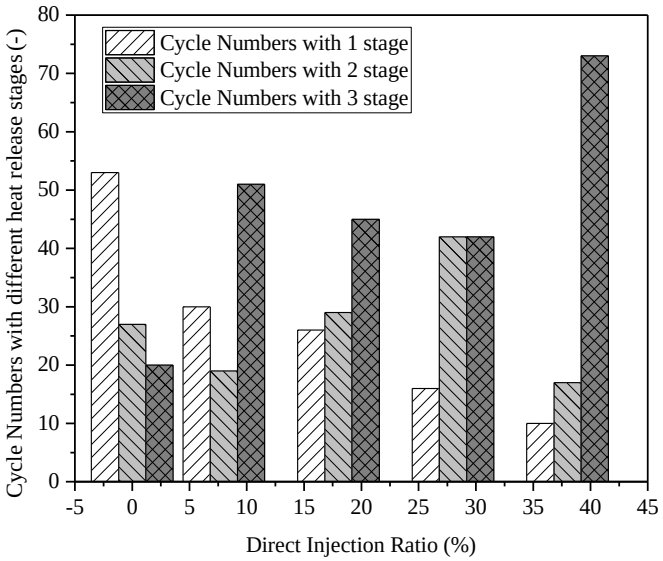

Figure 18. The variations of heat release stages with different direct injection ratios.

3.2.3. Optimization of dilution method in SFI strategy

In order to further improve the combustion stability and overall efficiency of SCHC with SFI strategy, the FPE points and the heat release rate in FP stage should be further optimized. As the advancing of combustion phasing and FPE points was mainly limited by the knock phenomenon, the replacement of a part of hot residual gas by cooled external EGR could be used to prohibit the knock phenomenon and advance the FPE point further. On the other hand,

due to the fact that a large amount of exhaust gas trapped in the cylinder could decrease the flame speed, the replacement of a part of residual gas by fresh air could further enhance the flame speed in the initial FP stage of SCHC with higher direct injection ratios, therefore improving the fuel efficiency. Therefore, the effects of external EGR and air dilution on the SCHC with SFI strategy were investigated in this section. During the experiments, the exhaust valve phasing was retarded 20 ºCA away from the combustion TDC to decrease the residual gas fraction from 12% to 7% and introduce the alternative external EGR or fresh air. Other experimental conditions, such as the exhaust valve lift, intake valve phasing and lift, the total fuel amount and engine speed, were kept as the same with previous experiments which have been detailed in Section 2. In the EGR dilution strategy, the 14% external cooled EGR was induced into the cylinder and the overall air-fuel ratio was kept stoichiometric. In the air dilution strategy, fresh air was used to dilute the combustion process and the excess air coefficient (lambda) was increased to 1.2. Those two dilution strategies were compared in this section to evaluate the optimization methods of SFI strategy.

Figure 19 compares the optimal spark timing and mean MPRR in top 50 cycles between EGR and air dilution strategy with different direct injection ratios at same engine load, speed and total fuel amount. The spark timing was advanced by using the EGR strategy due to the effect of cooled EGR on prohibiting the knock phenomenon. Compared to the EGR strategy, the air dilution strategy showed less impact on the optimal spark timing. The reason can be attributed to the enhancement of the early flame propagation due to the avoidance of over-rich region around the spark plug. In both EGR strategy and air dilution strategies, the fuel stratification at diluted and lean conditions could increase the heat release from flame propagation and induce

earlier auto-ignition combustion, which in turn led to higher MPRR. Therefore, it was found that the MPRR increased with direct injection ratio with almost constant spark timing in both EGR dilution and air dilution strategies.

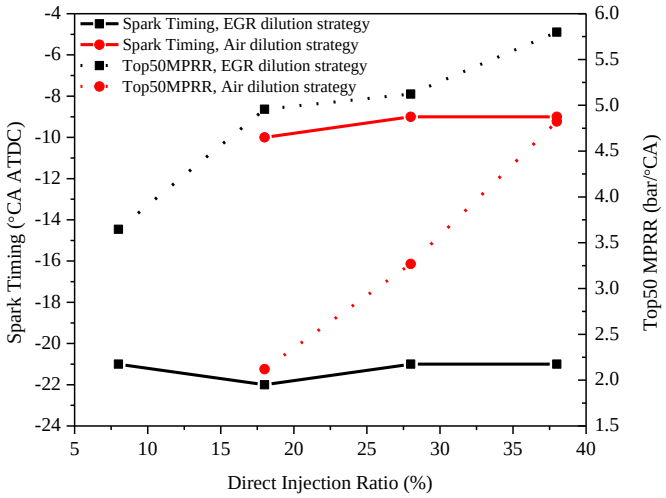

Figure 19. The comparison of spark timing and top50 MPRR between EGR and air dilution strategies with different direct injection ratios.

Figure 20 compares the CA10 and combustion duration between EGR and air dilution strategies with different direct injection ratios. It was found that the CA10 showed an advancing trend with direct injection ratio in the EGR dilution strategy, which was caused by the enhanced flame propagation with the stratified charge. However, the CA10 was almost constant with different direct injection ratios in the air dilution strategy. The reason can be attributed to the relatively later spark ignition timing and faster flame propagation process at each direct injection ratio with the air dilution strategy. It was found that the ignition delay between CA10 and spark timing (in Fig. 19) with the air dilution strategy was significantly shorter than that with the EGR dilution strategy. The combustion duration was decreased significantly with the increase of direct injection ratio with both EGR and air dilution strategies, indicating faster combustion process with the stratified charge in both dilution strategies.

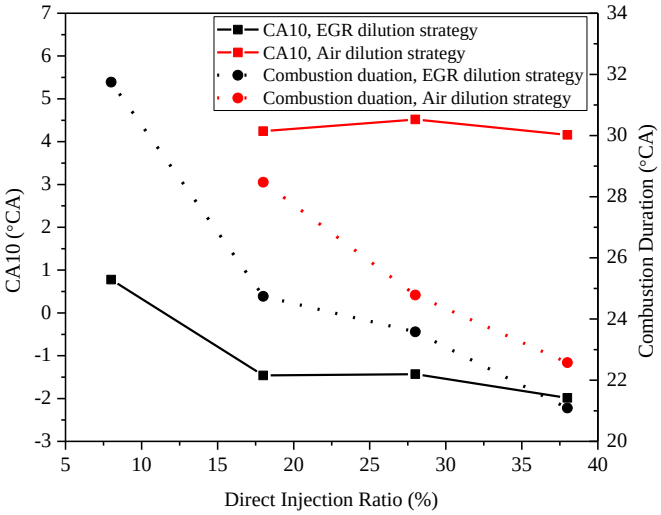

Figure 20. The comparison of CA10 and combustion duration between EGR and air dilution strategies with different direct injection ratios.

Figure 21 shows the variations of heat release stages in EGR and air dilution strategies with different direct injection ratios. As shown in the figure, the cycles with 1-stage heat release process was gradually reduced with the increase of direct injection ratio in both EGR and air dilution strategies. On the contrary, the combustion tended to be a 3-stage heat release process with the increase of direct injection ratio. Figure 21 also shows that the air dilution strategy produced more 3-stage heat release cycles than the EGR dilution strategy. When the direct injection ratio exceeded 18%, the number of the cycles with 3-stage heat release was more than 90 in 100 consecutive cycles in the air dilution strategy.

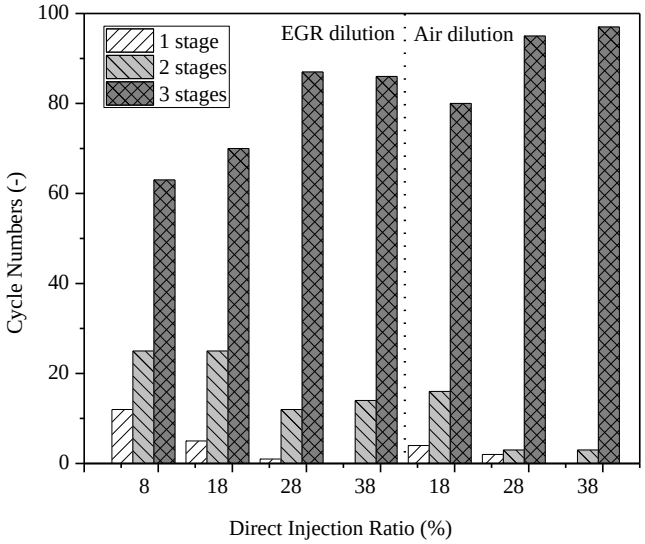

Figure 21. The variations of heat release stages in EGR and air dilution strategies with different direct injection ratios.

Figure 22 compares IMEP and COV of IMEP in EGR and air dilution strategies with different direct injection ratios. The replacement of a part of hot residual gas by EGR and air increased the IMEP significantly compared with the previous results with stoichiometric mixture without EGR (Fig. 14). However, the IMEP was gradually decreased with the direct injection ratio in both EGR and air dilution strategies. Compared with EGR dilution strategy, air dilution strategy produced higher IMEP at the same direct injection ratio. The COV of IMEP showed a decreasing trend with the direct injection ratio in both EGR and air dilution strategies except the serious knock operating point with the direct injection ratio of 38% in EGR dilution strategy. At this operating point, the advanced CA10 led to fast development of the combustion process with very high proportion of auto-ignition heat release, leading to the knocking combustion and negative work. The improved stability with the direct injection ratio can be attributed to the increased number of 3-stage heat release cycles, as shown in Fig. 21.

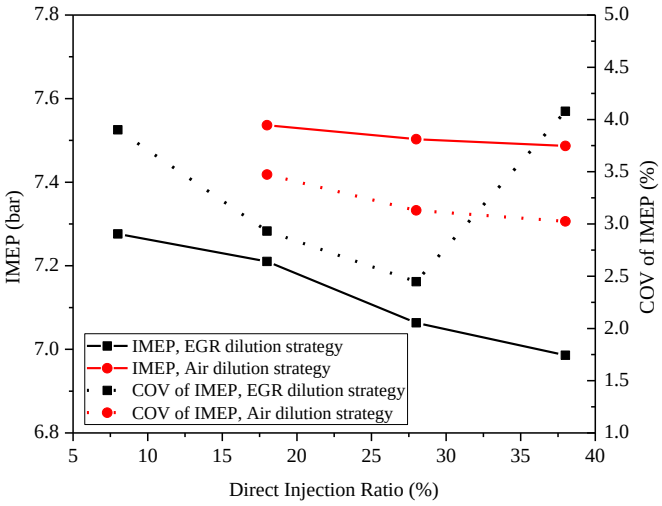

Figure 22. The comparison of IMEP and COV of IMEP in EGR and air dilution strategies with different direct injection ratios.

Figure 23 compares total heat release per cycle and CO emission in EGR and air dilution strategies with different direct injection ratios. As the air dilution strategy had higher oxygen concentration and specific heat ratio, the combustion process can be improved with higher total heat release and lower CO emission, as shown in Fig. 23. With the increase of direct injection ratio, the combustion was deteriorated with lower total heat release and higher CO emission in both EGR and air dilution strategies, which led to the decrease of IMEP. Overall, the relatively low direct injection ratio was found to be better to achieve optimal heat release process and higher thermal efficiency of SCHC.

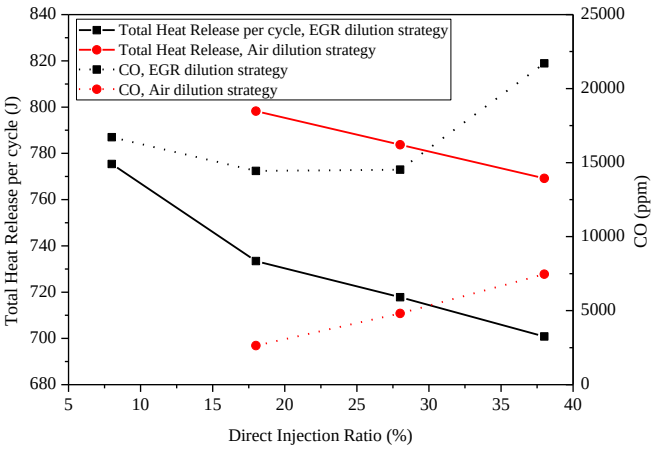

Figure 23. The comparison of total heat release per cycle and CO emission in EGR and air dilution strategies with different direct injection ratios.

Figure 24 compares the IMEP contour map against crank angles of FPE points and heat release rates in FP stage with different direct injection ratios in EGR and air dilution strategies. The contour maps of IMEP with the EGR dilution strategy extended to the left side (earlier FPE points) at the same direct injection ratio due to advanced combustion process. On the other hand, the contour map with the air dilution strategy moved toward the upper region (higher heat release rate in FP stage). As the results, both EGR and air dilution strategies could produce higher maximum IMEP compared with the stochiometric case without EGR. However, it should be noted that the maximum IMEP with direct injection ratio of 38% in the EGR dilution strategy was not located at the left-upper boundary due to the knock phenomena with over-fast heat release rate in FP stage at the boundary region, which also led to the deterioration of the maximum IMEP. Therefore, the knock phenomenon at the left-upper boundary should be avoided in the EGR dilution strategy in order to achieve higher thermal efficiency.

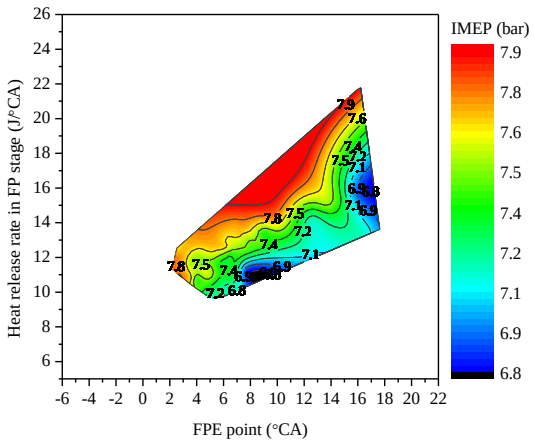

a) Direct injection ratio of 18%, air dilution strategy

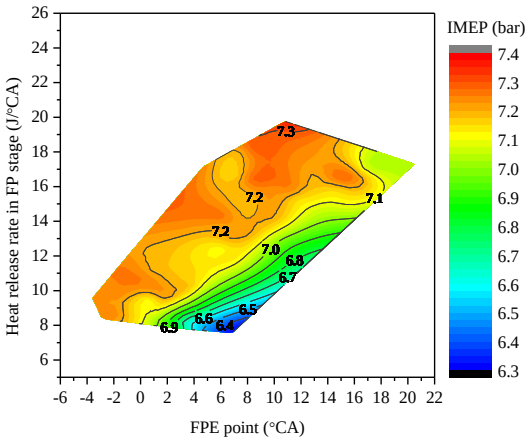

b) Direct injection ratio of18%, EGR dilution strategy

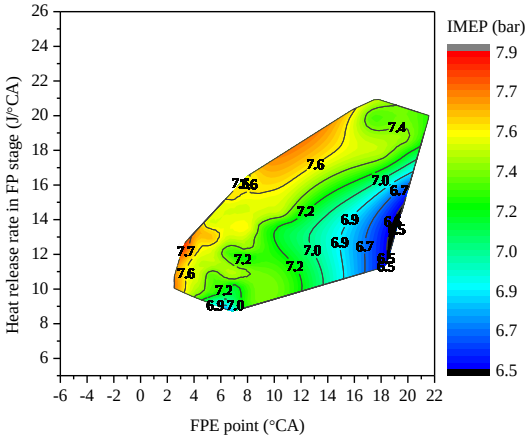

c) Direct injection ratio of 28%, air dilution strategy

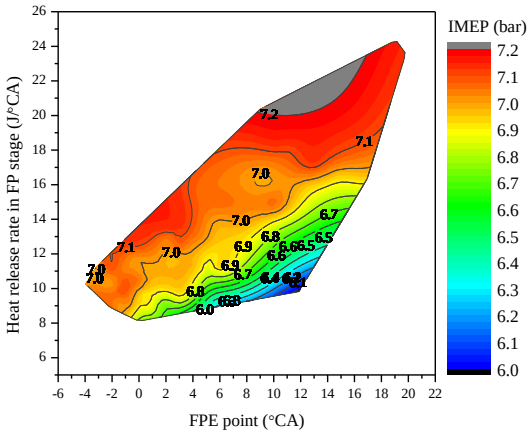

d) direct injection ratio of 28%, EGR dilution strategy

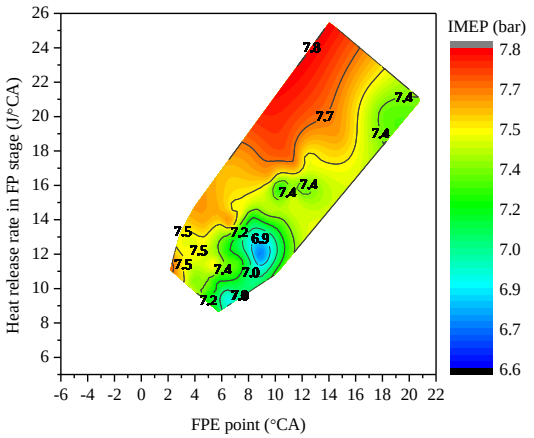

e) Direct injection ratio of 38%, air dilution strategy

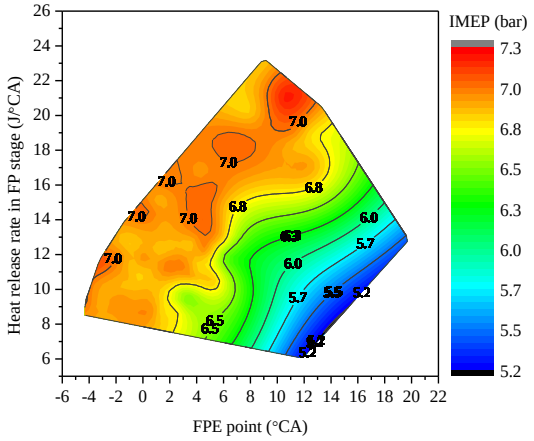

f) Direct injection ratio of 38%, EGR dilution strategy

Figure 24. The comparison of IMEP contour map against crank angles of FPE points and heat release rates in FP stage with different direct injection ratios in EGR and air dilution strategies.

Figure 25 shows the statistic information of FPE points and the heat release rates in FP stage between EGR and air dilution strategies. It can be found that the distribution of FPE points among different cycles in air dilution strategy was more concentrated than that in EGR dilution strategy. There were only slight variations of the mean and median values of the FPE points with different direct injection ratios in air dilution strategy. In comparison, the mean and median values of FPE points in EGR dilution strategy showed an advancing trend with the increase of the direct injection ratio except the case with direct injection ratio of 38%. Therefore, the EGR

dilution strategy showed stronger capability to advance the FPE points. As shown in Figure 25 (b), the air dilution strategy showed higher mean and median values of heat release rates in FP stage than the EGR dilution strategy with different direct injection ratios. The comparison between Fig. 25 and Fig. 17 indicated that the application of EGR and air dilution strategies could produce earlier FPE points, higher heat release rate in FP stage and more concentrated distribution patterns than the stoichiometric case without EGR, therefore having better ability to improve both combustion efficiency and stability.

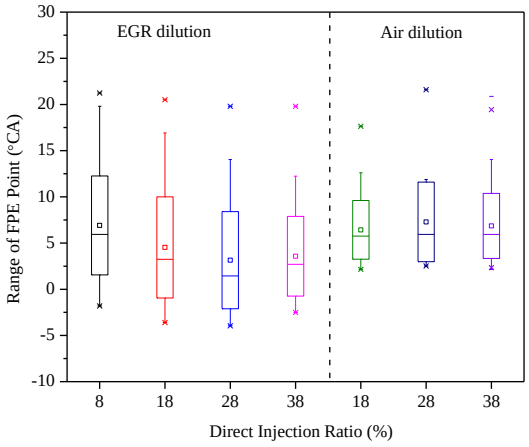

a) crank angles of FPE points

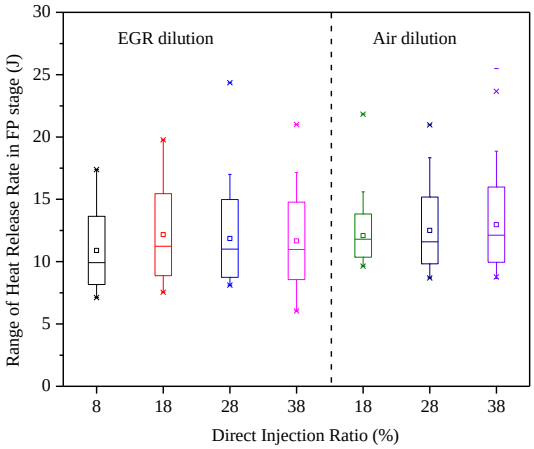

b) heat release rates in FP stage

Figure 25. The statistic information of FPE points and the heat release rates in FP stage between EGR and air dilution strategies.

4. Summary and conclusions

In this research, the heat release characteristics of the SI-CAI hybrid combustion with SFI strategy and its control methods were investigated in detail in a single cylinder gasoline 4-stroke engine equipped with variable valve lift and timing control devices. The main findings can be summarized as follows:

(1) The SI-CAI hybrid combustion exhibit significant cycle-to-cycle variations of the heat release process, leading to high MPRR in some cycles while low efficiency in others.

(2) The blend method (BM) was developed to demarcate different heat release stages of SCHC by combining the SOD method and Wiebe function fitting method. Based on the assumption of the 3-stage heat release in SCHC, the Wiebe function fitting method was used to judge the transition periods, while SOD was used to scan the local extreme points within transition periods and identify the transition points.

(3) Although the overall MPRR of SCHC was much less than 5 bar/ºCA, there still could be a considerable amount of knock cycles due to large variations of heat release process. Therefore, it was proposed that the mean MPRR of top 50 cycles in 100 consecutive cycles should be controlled less than 5 bar/ºCA and MPRR below 10 bar/ºCA in order to avoid the knock.

(4) The earlier FPE point and higher heat release rate in FP stage produced higher IMEP at the same amount of fuel per cycle, therefore improving the fuel economy of SCHC.

(5) Compared with the homogenous case, the SFI strategy led to wider contour map of IMEP toward earlier FPE point and higher heat release rate in FP stage. With the

increase of direct injection ratio in SFI strategy, the spark timing could be advanced to improve the efficiency due to the reduced MPRR. The number of the cycles with 1-stage heat release and the variation of the combustion process were decreased with the increase of direct injection ratio in SFI strategy. However, the high direct injection ratio would result in the decrease of combustion efficiency and total heat release per cycle.

(6) The EGR and air dilution strategies could expand the contour map of IMEP toward the earlier FPE point and higher heat release rate in FP stage, therefore improving thermal efficiency of SFI combustion. Although a higher direct injection ratio could decrease the combustion duration and the variation of heat release process of SCHC in both EGR and air dilution strategies, a relatively low direct injection ratio was found to be better to improve the thermal efficiency of SCHC. Compared to EGR dilution strategy, the air dilution strategy showed a distinct advantage on thermal efficiency.

Funding

This work was supported by Project of National Key Basic Research Plan (grant number 2013CB228403) from the Ministry of Science and Technology; and Project of National Nature Science Foundation of China (grant number 51206118) from National Nature Science Foundation Committee of China.

References

1. Zhao H., (Ed.) Homogeneous Charge Compression Ignition (HCCI) and Controlled Autoignition (CAI) Combustion Engines for Automotive Industry, ISBN 1845691288

2. Chen T., Xie H., Li L.,et al., Continuous Load Adjustment Strategy of a Gasoline HCCI-SI Engine Fully Controlled by Exhaust Gas. SAE Paper 2011-01-1408, 2011

3. Li L., Xie H., Chen T., Yu W. et al., Experimental Study on Spark Assisted Compression Ignition (SACI) Combustion with Positive Valve Overlap in a HCCI Gasoline Engine, SAE Technical Paper 2012-01-1126, 2012, doi:10.4271/2012-01-1126.

4. Persson H., Hultqvist A., Johansson B., et al, Investigation of the Early Flame Development in Spark Assisted HCCI Combustion Using High Speed Chemiluminescence Imaging [C], SAE Paper 2007-01-0212, 2007

5. Weinrotter M., Wintner E., Iskra K., et al., Optical Diagnostics of Laser-Induced and Spark Plug-Assisted HCCI Combustion, SAE Paper 2005-01-0129

6. Hyvönen J., Haraldsson G. and Johansson B., Operating Conditions Using Spark Assisted HCCI Combustion During Combustion Mode Transfer to SI in a Multi-Cylinder VCR-HCCI Engine, SAE Technical Paper 2005-01-0109, 2005

7. Wang Z., He X., Wang J., et al, Combustion visualization and experimental study on spark induced compression ignition (SICI) in gasoline HCCI engines [J], *Energy Conversion and Management* 51 (2010), 908?17

8. Manofsky L., Vavra J., Assanis D. and Babajimopoulos A., Bridging the Gap between HCCI and SI: Spark-Assisted Compression Ignition [C], SAE Paper 2011-01-1179, 2011

9. Zhao H (ed.) Homogeneous Charge Compression Ignition (HCCI) and Controlled Autoignition (CAI) combustion engines for automotive industry. Cambridge: Woodhead

Publishing Limited, 2007.

10. Wagner R., Edwards K., Daw C., et al., On the Nature of Cyclic Dispersion in Spark Assisted HCCI Combustion [C], SAE Paper 2006-01-0418, 2006.

11. Daw S., Edwards K., Wagner R., et al, Modeling cyclic variability in spark-assisted HCCI [C], *Proceedings of the ASME Internal Combustion Engine Division 2007 Fall Technical Conference*, ICEF2007-1685, 2007.

12. William G., Wagner R., Edwards D., Daw S., Analysis of cyclic variability in spark-assisted HCCI combustion using a double Wiebe function [J], *Proceedings of the Combustion Institute* 32 (2009) 2885-2892.

13. Chen T., Zhao H., Xie H. and He B., Analysis of cyclic variations during mode switching between spark ignition and controlled auto-ignition combustion operations, International Journal of Engine Research 2015, 16 (3), 356-365.

14. Bunting B.G., Combustion, Control, and Fuel Effects in a Spark Assisted HCCI Engine Equipped with Variable Valve Timing [C], SAE Paper 2006-01-0872, 2006

15. Yun H., Wermuth N., Najt P., Extending the High Load Operating Limit of a Naturally-Aspirated Gasoline HCCI Combustion Engine [C], SAE Paper 2010-01-0847, 2010

16. Chang Y., Wooldridge M., and Bohac S., Extending the Dilution Limit of Spark Ignition Combustion via Fuel Injection during Negative Valve Overlap, SAE Technical Paper 2016-01-0671, 2016, doi:10.4271/2016-01-0671.

17. Polovina D., McKenna D., Wheeler J., Sterniak J. et al., Steady-State Combustion

Development of a Downsized Multi-Cylinder Engine with Range Extended HCCI/SACI Capability, *SAE Int. J. Engines 6(1)*:2013, doi:10.4271/2013-01-1655.

18. Yang C.H. and Zhao H., In-cylinder studies of hybrid combustion in a direct injection single-cylinder optical engine, Int. J. Engine Res. Vol. 11, JER 519, 515-531, 2010, doi: 10.1243/14680874JER519

19. Aroonsrisopon T. et al., A Computational Analysis of Direct Fuel Injection During the Negative Valve Overlap Period in an Iso-Octane Fueled HCCI Engine, SAE Technical Paper 2007-01-0227.

20. Wheeler J., Polovina D., Ramanathan S., Roth K. et al., Increasing EGR Tolerance using High Tumble in a Modern GTDI Engine for Improved Low-Speed Performance, SAE Technical Paper 2013-01-1123, 2013, doi:10.4271/2013-01-1123.

21. Xie H., Xu K., Wan M., Chen T. and Zhao H., Investigations into the influence of internal and external exhaust gas recirculation on the combustion stability in an optical gasoline spark ignition engine, Proc IMechE Part D: J Automobile Engineering 2015, Vol. 229(11) 1514–1528.

22. Persson H., Hultqvist A., Johansson B., and Remón A., Investigation of the Early Flame Development in Spark Assisted HCCI Combustion Using High Speed Chemiluminescence Imaging, SAE Technical Paper 2007-01-0212, 2007

23. Olesky L.M., Martz J.B, et al, The effects of spark timing, unburned gas temperature, and negative valve overlap on the rates of stoichiometric spark assisted compression ignition combustion, *Applied Energy* 105 (2013) 407–417

24. Hellstrom E., Stefanopoulou A., V´avra J.,et al. Understanding the dynamic evolution of cyclic variability at the operating limits of HCCI engines with negative valve overlap. SAE Technical Paper 2012-01-1106, 2012

25. Shi X., Chen J.-Y., and Chen Z. (2015). Numerical study of laminar flame speed of fuel-stratified hydrogen/ air flames. *Combustion and Flame*, 163, 394–405. 2015.10.014

26. Shi X. and Chen J. (2017). Numerical analysis and model development for laminar flame speed of stratified methane/air mixtures. *Combustion and Flame*, 184, 233–245.

27. Shi X., Chen J. Y. and Chen Y. (2017). Laminar flame speeds of stratified methane, propane, and n-heptane flames. *Combustion and Flame*, 176, 38–47.

28. Wang X., Zhao H., Xie H. and He B., Numerical Study of the Effect of Piston Shapes and Fuel Injection Strategies on In-Cylinder Conditions in a PFI/GDI Gasoline Engine, SAE Int. J. Engines 7(4):2014, doi:10.4271/2014-01-2670.

29. Wang X., Zhao H., Xie H., Effect of piston shapes and fuel injection strategies on stoichiometric stratified flame ignition (SFI) hybrid combustion in a PFI/DI gasoline engine by numerical simulations, Energy Conversion and Management 98 (2015) 387–400.

30. Xie H., Hou S., Qin J., et al, Control Strategies for Steady and Transient Operation of a 4-Stroke Gasoline Engine with CAI Combustion using a 4-Variable Valve Actuating System (4VVAS), SAE Paper 2006-01-1083.

Appendix

Notation

AI	auto-ignition
AIP	auto-ignition peak
AIB	auto-ignition beginning
BM	blend method
CA10	crank angle at 10% burned mass
CA80	crank angle at 80% burned mass
CA95	crank angle at 95% burned mass
CAI	controlled auto-ignition
CC	complicated combustion
CO	carbon monoxide
COV	coefficient of variation
EGR	exhaust gas recirculation
FP	flame propagation
FPE	flame propagation ending
HC	hydrocarbons
HCCI	homogenous charge compression ignition
IMEP	indicated mean effective pressure
IQR	likely range of variation
MHRR	maximum heat release rate
MPRR	maximum pressure rise rate
NO_X	nitrogen oxides
NVO	negative valve overlap
RGF	residual gas fraction
SCHC	SI-CAI hybrid combustion
SFI	stratified flame ignited
SI	spark ignition
SOD	second order derivative
TDC	top dead center
Top50 MPRR	mean MPRR of top 50 cycles in 100 consecutive cycles